Beyond the static corrugation model: dynamic surfaces with the embedded atom method

Smits, B.; Somers, M.F.

The Journal of Chemical Physics

Beyond the static corrugation model: Dynamic surfaces with the embedded atom method

Cite as: J. Chem. Phys. **154**, 074710 (2021); https://doi.org/10.1063/5.0036611
Submitted: 06 November 2020 • Accepted: 21 January 2021 • Published Online: 18 February 2021

B. Smits and M. F. Somers

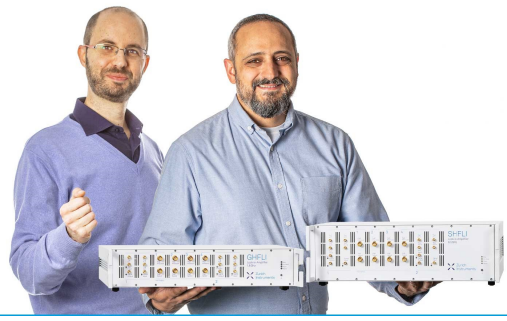

The Journal of Chemical Physics ARTICLE scitation.org/journal/jcp

Beyond the static corrugation model: Dynamic surfaces with the embedded atom method

Cite as: J. Chem. Phys. 154, 074710 (2021); doi: 10.1063/5.0036611
Submitted: 6 November 2020 • Accepted: 21 January 2021 •
Published Online: 18 February 2021

B. Smits and M. F. Somers[a)]

AFFILIATIONS

Leiden Institute of Chemistry, Gorlaeus Laboratories, Leiden University, RA Leiden 2300, The Netherlands

[a)]Author to whom correspondence should be addressed: m.somers@chem.leidenuniv.nl

ABSTRACT

The D_2 on Cu(111) system has for many years been one of the major benchmark systems for surface scientists. Generating surface configurations using the embedded atom method (EAM), we investigate the quality of the chemically accurate static corrugation model (SCM) for including surface temperature effects, with a focus on the random displacement approach to its distorted surface generation. With this EAM potential, we also treat the Cu(111) surface of our system fully dynamically and shine a further light on not only the quality of the SCM sudden approach but also the limited effect of energy exchange with the surface. Reaction and (in)elastic scattering probability curves, as well as simulated time-of-flight spectra, show good agreement with both earlier works and experimental results, with surface reactions showing a preference for surface atoms displaced away from the incoming molecule. The good agreement with the non-static surface model also further establishes the limited effect of energy exchange on not only the reaction but also on the elastic and inelastic scattering probabilities, even though some molecular translational energy is deposited into the surface.

I. INTRODUCTION

For many years, theoreticians and experimentalists have been working on describing gas–solid surface reactions.[1–3] These are especially of interest due to their importance in many (industrial) processes, such as the Haber–Bosch process[4] or H_2 dissociation for hydrogen engines.[5] To best describe these processes, the reaction mechanisms are broken up into simple elementary reaction steps. Studying of individual steps would then allow for a very accurate description of the full catalytic process.

Our system of choice for this work is the D_2 dissociation on a Cu(111) surface. This system is one of the model systems for surface scientists, with much available experimental[6–12] and theoretical[2,13–18] data. In the past, theoretical work was often performed using the Born–Oppenheimer and the static surface (BOSS) approach, where surface atoms are assumed to be fully static, and the electron and nucleus dynamics are assumed to be separated. Here, the *ab initio* density functional theory (DFT) results are often fit to a 6D potential energy surface (PES) using an approach such as the corrugation reducing procedure (CRP).[19]

Making use of this method, Díaz *et al.* developed the specific reaction parameter (SRP) approach.[13] Linearly combining two different DFT functionals, one overestimating and one underestimating the dissociation barrier, this work was able to reproduce experimental molecular beam experiments of H_2 of Cu(111) with an error of less than 1.0 kcal/mol.[20]

Although good results were obtained using these methods, the surface slab was kept at its ideal, 0 K configuration, whereas experiments are often performed at higher temperatures.[21] To allow for the PES to take into account surface temperature effects, Wijzenbroek and Somers coined the static corrugation model (SCM).[22] In this model, surface slab atoms are displaced from the ideal lattice but kept static. It was theorized that such an approach would work well for a H_2 and D_2 on copper system, which is expected to have only limited energy transfer both due to the mass mismatch between hydrogen and copper atoms and the relatively slow speed of the thermally equilibrated copper surface atoms. A two body (H–Cu) coupling potential (V_{coup}) was introduced to describe the changes in the PES due to these displacements. This coupling potential was fitted to a dataset of surface configurations obtained using SRP48

DFT calculations.[16] This initial approach to the SCM showed great agreement with *ab initio* molecular dynamics (AIMD) calculations using the same DFT functional.[16] Furthermore, it resulted in better agreement with experiment than originally achieved with the SRP-BOSS approach, although the limited size of the dataset also showed a sizable error in the H–Cu coupling potential. To improve upon the SCM, Spiering *et al.* expanded the SCM to an effective three-body potential by including the H–H distance into the coupling potential.[23] Furthermore, the dataset for fitting was greatly expanded, which reduced the RMSE of the fitted three-body coupling potential to 29.4 meV, compared to 66.6 meV for the two-body potential as described in the initial work. To generate these SCM statically distorted surface slabs, each atom is displaced using a normal distribution based on an experimentally determined Debye–Waller factor for a specific modeled temperature, with interlayer distances taken directly from experiment. It is, however, still unclear if such a random displacement generates physically relevant surface slabs.

Several other approaches to (statically) including surface temperature effects have been shown to be successful for a variety of gas–metal systems, such as the reactive force-field (RFF) approach by Busnengo and co-workers [H_2/Pd(111)[24], CO/Cu(110), and CH_4/Pt(110)[25,26]], the reaction path Hamiltonian approach (RPH) by Jackson and co-workers (CH_4 on Ni and Pt[27–31]), as well as high-dimensional AIMD with a moving surface.[16,32] In general, each of these approaches relies on (a fit of) the DFT results to describe the effect of the distorted surface on the incoming reactant, similar to the SCM. Of particular interest is the RPH work by Jackson *et al.* as they show the relative accuracy of the sudden approach, of which the SCM is a variant, when dealing with simple systems.[31]

Another approach to including surface temperature effects and even dynamic surfaces that we would like to mention here is the high-dimensional neural network potential (HD-NNP), which has seen a rise in applications within the field of theoretical surface science.[33,34] The very nature of the high dimensional neural network approaches, however, also comes with challenges: one needs exactly the right dataset to train such a network for specific uses and one should take care of not "extrapolating" beyond that dataset. Advanced symmetry functions are often needed to make such high dimensional NN stable and accurate and to display the right physics, and especially important for quantum dynamics, these high dimensional NN could introduce small artifacts into the PES if the training set is not dense enough.[35]

Therefore, we elected to expand upon the SCM approach by generating surface slabs using a highly accurate embedded atom method (EAM) potential as described by Sheng *et al.*[36] This potential has been shown to accurately describe not only lattice constants and phonon dispersion curves but also thermal expansion of the bulk metal and the FCC copper surface slabs. These surface slabs can then be used in combination with the SCM coupling potential to generate dissociation curves and simulated time-of-flight spectra. A comparison of these curves between these randomly displaced surfaces and EAM generated surfaces should then allow us to validate the quality of this earlier work.

To further expand our model, we can even use the EAM potential to dynamically describe our copper surface during dissociation simulations. Here, the SCM coupling potential not only describes the effect of the surface on the D_2 but also describes the effect of the D_2 on the surface, effectively allowing for energy exchange to be introduced in our system. Energy exchange has long be theorized to not be very relevant for dissociation probabilities in the H_2 on Cu(111) system due to the large mass mismatch. In this work, however, we will be able to investigate its effect directly by comparing results from both a static and a dynamic surface using exactly the same potentials.

In contrast to an HD-NNP approach, which would need a new extended training set and fit if one switches to another facet or to a stepped surface, the approach we follow here only requires a new CRP BOSS PES. The V_{coup} and EAM potentials are generic in that respect as it has been shown that the underlying DFT function of V_{coup} is transferable between the H_2 on Cu(111) and H_2 on Cu(100) systems.[22,68] Moreover, recently, a H_2 on Cu(211) stepped CRP BOSS PES has been constructed also with the SRP48 DFT functional.[37,38]

The transferability of the SCM approach to surface slabs of a different transition metal, such as Pt or Ag, will still require additional work. However, this can be greatly reduced by using one of the many (CRP) PESs[3] and EAM potentials[36] available in the literature, reducing it to merely fitting a new SCM coupling potential. Of special interest would be those systems with an early barrier as they exhibit a relatively small amount of corrugation and a large mass mismatch between the D_2 and the metal. For those systems where no well performing GGA-level DFT functionals are available, such as Pd,[39] another first principles approach would be required to obtain a dataset to fit the SCM coupling potential, as is also the case for HD-NNPs, which generally require extensive DFT datasets.[35]

In this work, however, we aim to investigate two assumptions made in previous works. Primarily, we will validate the physical relevance of the SCM random displacement approach to surface slab generation by comparing the results of D_2 dissociation on such a surface slab to a physically accurate surface slab generated with an EAM potential. Furthermore, we also go beyond the SCM by dynamically treating the metal atoms of the surface slab with this EAM potential. This will allows us to both further investigate the quality of the sudden approximation that lies at the base of the SCM as well as investigate the importance of energy exchange with the Cu surface for chemisorption and (in)elastic scattering probabilities.

II. METHOD

A. Static corrugation model

The static corrugation model (SCM) was designed to improve upon perfect lattice BOSS dynamics by including surface temperature effects due to surface atom displacements. This is achieved by expanding the description of the potential energy surface (PES) into three terms.[22] In addition to the potential for the ideal, static surface, $V_{DFT}(\vec{q}_{id}, \vec{r})$, the two additional terms V_{strain} and V_{coup} are included to describe the internal strain of the surface due to distortion and the change in surface–adsorbate interaction due to surface atom displacement, respectively. Thus, the total PES can be described as

$$V_{DFT}(\vec{q}, \vec{r}) = V_{DFT}(\vec{q}^{\,id}, \vec{r}) + V_{coup}(\vec{q}^{\,id} \to \vec{q}, \vec{r}) + V_{strain}(\vec{q}^{\,id} \to \vec{q}), \quad (1)$$

where $\vec{q}$ describes the positions of all surface atoms, $\vec{q}_{id}$ describes the ideal lattice positions of all surface atoms, and $\vec{r}$ describes the positions of all adsorbed atoms.

Under the assumption of a static surface, V_{strain} can be neglected as it will not change during dynamics. Thus, the full dimensional DFT PES of our distorted system can be approximated as

$$V_{DFT}(\vec{q},\vec{r}) \approx V_{SCM}(\vec{q}^{\,id} \to \vec{q},\vec{r}) = V_{DFT}(\vec{q}^{\,id},\vec{r}) + V_{coup}(\vec{q}^{\,id} \to \vec{q},\vec{r}). \quad (2)$$

A continuous representation of V_{coup} is required to do dynamical simulations. For $V_{DFT}(\vec{q}^{\,id},\vec{r})$, many approaches to obtaining such a description have been described, with some examples found in Refs. 19, 34, and 40.

The main focus of previous work on the SCM has been obtaining a continuous description of V_{coup}. This was achieved through interpolation of a collection of DFT data using the CRP approach[19] and fitting this to the functional form

$$V_{coup}\left(\vec{r},\vec{q}^{\,id} \to \vec{q}\right) = \sum_i^{\vec{r}} \sum_j^{\vec{q}} \left[V_{H\text{-}Cu}(|\vec{r}_i - \vec{q}_j|) - V_{H\text{-}Cu}(|\vec{r}_i - \vec{q}_j^{\,id}|) \right] \quad (3)$$

with $\vec{r}_i$ to describe the positions of adsorbate i and $\vec{q}_j$ to describe the surface atom position j. This appears similar to a previous study by Pineau *et al.*, who employed this approach to describe the relaxation of hot atoms on a metal surface.[41] However, while Pineau *et al.* directly employed the 1D CRP function to approximate the coupling terms of the V_{coup}, Wijzenbroek and Somers instead elected to fit V_{coup} from raw DFT data using a separate switched Rydberg-like function,[22]

$$V_{H\text{-}Cu}(R) = (1-\rho(R))V(R) + \rho(R)V(P_7) \quad (4)$$

with

$$V(R) = -e^{-P_4(R-P_5)}\left(\sum_{k=0}^{3} P_k (R-P_5)^k\right) \quad (5)$$

and

$$\rho(R) = \begin{cases} 0 & \text{for } R < P_6 \\ \frac{1}{2}\cos\left(\frac{\pi(R-P_7)}{P_7-P_6}\right) + \frac{1}{2} & \text{for } P_6 \le R \le P_7 \\ 1 & \text{for } R > P_7. \end{cases} \quad (6)$$

The SCM was later expanded by Spiering *et al.* to include an effective three-body potential.[23] This was achieved by making each fitting parameter P_i linearly dependent on the distance between the two adsorbates r_{H-H},

$$P_i = \begin{cases} P_{i,a} r_{H-H}^{min} + P_{i,b} & \text{for } r_{H-H} < r_{H-H}^{min} \\ P_{i,a} r_{H-H} + P_{i,b} & \text{for } r_{H-H}^{min} \le r_{H-H} \le r_{H-H}^{max} \\ P_{i,a} r_{H-H}^{max} + P_{i,b} & \text{for } r_{H-H} > r_{H-H}^{max}. \end{cases} \quad (7)$$

Here, the cut-off values r_{H-H}^{max} and r_{H-H}^{min} are obtained from, respectively, the largest and smallest values of r_{H-H} used during the fitting procedures.

To account for thermal expansion effects while using the CRP potential of the system for an ideal lattice, the H_2 CoM vectors are linearly contracted or stretched along the lattice vectors u and v. By stretching along the lattice vectors instead of the x- or y-vectors, accidental introduction of extra artificial vibrational or rotational strain is avoided. Thus, the full effective SCM potential becomes

$$V_{SCM}(\vec{r},\vec{q},\vec{q}^{\,id}) = V_{CRP}(\vec{r}^{\,id}(\vec{r}),\vec{q}^{\,id}) + \sum_i^{\vec{r}} \sum_j^{\vec{q}} \left[V_{H\text{-}Cu}(|\vec{r}_i - \vec{q}_j|) - V_{H\text{-}Cu}(|\vec{r}^{\,id}(\vec{r}) - \vec{q}_j^{\,id}|) \right], \quad (8)$$

where $\vec{r}^{\,id}(\vec{r})$ scales the H_2 CoM vectors along the lattice coordinates.[23]

B. Embedded atom method

First described by Daw and Baskes in 1983,[42] the embedded atom method (EAM) has been a strong tool for theoretical surface scientists. The EAM is based on the quasiatom,[43] or effective medium,[44] approach, which was designed to describe impurities in metals.[45] Here, an impurity, such as a small atom, embedded in the metal is modeled as a particle in a uniform environment of electron density. The EAM, instead, takes it one step further, treating each surface atom as the "impurity" in an electron density obtained from contributions of each of the neighboring atoms. Each atom would thus get an embedding energy, which is defined as the difference in energy between the atom inside the uniform electron density associated with its neighbors and that of the same atom in a vacuum. The total sum of each individual atomic energy is then approximated as the total (potential) energy of the metal,

$$E_{tot} = \sum_i F_i(n_i), \quad (9)$$

where F_i is the so-called embedding energy of atom i and n_i is the density this atom experiences at position r_i.

This initial approach to the EAM did not perform as well as was expected, yielding unrealistic properties for solids due to the neglect of core–core repulsion and the "assumption of extreme locality."[45] Thus, a second, short-range pair interaction was added to the model to yield a total energy given by

$$E_{tot} = \sum_i \left[F_i(n_i) + \frac{1}{2} \sum_{j \ne i} \phi_{ij}(R_{ij}) \right]. \quad (10)$$

Here, ϕ_{ij} describes the pair interaction potential between atoms i and j, R_{ij} being the distance between the two. In this work, we will use another pair interaction to approximate the density n_i of atom i using

$$n_i = \sum_{j \ne i} \rho_{ij}(R_{ij}), \quad (11)$$

where ρ_i yields the density contribution of atom j to the density of atom i.

Thus, the EAM can be used to describe a (metal) system using a total of three functions: the pair function ϕ, the embedding function F, and the density function ρ.

We can combine this EAM potential with the SCM-modified DFT potential as described in Eq. (1) to obtain the full potential for a dynamic H_2 on Cu system. Here, we use the EAM potential to describe the strain in the surface (V_{strain}), the H_2 + Cu(111) CRP BOSS PES to describe the ideal static surface at 0 K, and the SCM coupling potential to describe the interaction between the two. This yields us the total potential of a fully dynamic H_2 on Cu(111) system,

$$\begin{aligned} V_{Dyn}(\vec{r}, \vec{q}, \vec{q}^{\,id}) = V_{CRP}(\vec{r}^{\,id}(\vec{r}), \vec{q}^{\,id}) \\ + \sum_i^{\vec{r}} \sum_j^{\vec{q}} \Big[V_{H\text{-}Cu}(|\vec{r}_i - \vec{q}_j|) \\ - V_{H-Cu}(|\vec{r}^{\,id}(\vec{r}) - \vec{q}_j^{\,id}|) \Big] \\ + \sum_k^{\vec{q}} \left[F_k \left(\sum_{l \neq k}^{\vec{q}} \rho_{kl}(|\vec{q}_k - \vec{q}_l|) \right) \right. \\ \left. + \frac{1}{2} \sum_{l \neq k}^{\vec{q}} \phi_{kl}(|\vec{q}_k - \vec{q}_l|) \right]. \end{aligned} \tag{12}$$

In this work, we will be using the cubic spline fits to F, ρ, and ϕ of the EAM potential as described by Sheng *et al.*[36] This highly accurate potential has been shown to reproduce a variety of experimental data and has been extensively used in other works.[46–49]

C. Quasi-classical dynamics of D_2 on Cu(111)

The CRP PES (V_{CRP}), its SCM variant (V_{SCM}), or its dynamic surface variant (V_{Dyn}) can be used to describe the interaction of an H_2 or D_2 molecule on an ideal, non-ideal, or dynamic Cu(111) surface, respectively. This CRP PES was fitted by Mondal *et al.*[14] and based on the SRP48 functional designed by Nattino *et al.*,[16] while the three-body SCM potential was fitted by Spiering *et al.*[23] with a dataset obtained from DFT using the same functional. As the name suggests, the exchange–correlation energy of the SRP48 functional is obtained from a weighted combination of the Revised Perdew–Burke–Ernzerhof (RPBE)[50] and Perdew–Burke–Ernzerhof (PBE)[51] functional, with 0.48:0.52 ratio. Although no van der Waals (vdW) correction is included in this approach, a previous comparison of SRP48 with a vdW corrected functional (optPBE-vdW)[52] has not shown any significant improvements for the H_2/D_2 on Cu(111) system.[18]

As we cannot investigate the quality of a PES directly, we will instead focus on the dissociative chemisorption and the (in)elastic scattering of these particles on our model surface using quasi-classical (QC) dynamics. In contrast to classical dynamics, quasi-classical dynamics also takes into account the presence of the zero-point energy of the initial rovibrational states, which has been shown to be important for properly describing the system.[2]

The initial conditions of the adsorbate are generated by first calculating the initial rovibrational energy levels for our chosen PES using the Fourier grid Hamiltonian method.[53] The diatomic molecule is then propagated with a constant time step in the vacuum for one full vibrational phase while recording both the positions and momenta of each atom. This allows us to obtain the QC distribution of r_{H-H} and the corresponding classical momenta.

Both the molecular angles with the surface, θ and ϕ, are chosen from a uniformly random distribution between [0, π] and [0, 2π], respectively. Internal angular velocities are chosen according to the quantized angular momentum $L^2 = J(J+1)\hbar^2$. The normal incidence momentum is chosen according to the initial incidence energy. The angle θ_L between the angular momentum vector and the surface normal is chosen randomly but constrained by $\theta_L = \pi$ for $J = 0$ and $\cos(\theta_L) = m_j/\sqrt{J(J+1)}$ if $J \neq 0$.

The initial adsorbate CoM position in Z is shifted 7 Å away from the surface, while the U (= $X - Y/\sqrt{3}$) and V (= $2Y/\sqrt{3}$) coordinates are chosen randomly from a uniform distribution between 0 and a, with a being the lattice constant of the surface slab (Fig. 1).

The surface slab atom positions of both the ideal and distorted lattices are required to obtain the SCM potential. The ideal lattice is constructed similar to that of the DFT slab used when constructing the CRP PES. Only those atoms within 16 bohrs of the CoM projection on the xy-plane are included.

The distorted lattice is instead constructed in two steps. First, the ideal lattice positions are expanded along the lattice axes u and v using the experimental lattice expansion factor.[54] The interlayer distances are similarly set to experimental results.[55] Then, each surface atom is distorted using a Monte Carlo approach, where the magnitude of the distortion is obtained from a Gaussian distribution with a width based on the temperature dependent Debye–Waller factor, as we will discuss in Sec. II D.

For distorted lattices generated with the EAM, the SCM expansion coefficient is instead calculated as the ratio between the ideal CRP lattice constant and the calculated EAM lattice constant. For these slabs, we similarly only take those slab atoms within 16 bohrs of the center of the surface slab, where (x, y, z) = (0, 0, 0).

By applying the EAM potential to our, in regular SCM, static surface, we can also perform surface dynamics with a dynamic surface. Here, the CRP and SCM approach describe the dynamics of

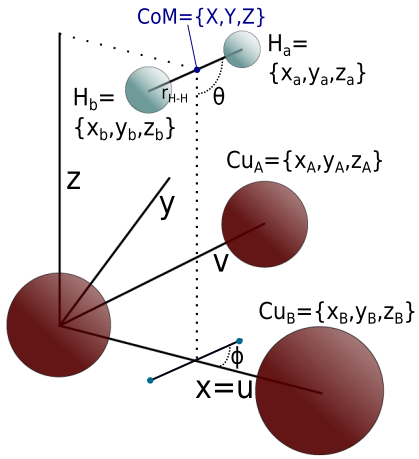

FIG. 1. Coordinate system of our incoming H_2 (light-blue) with lattice vectors for the Cu(111) surface slab (dark red). The 6 DoFs of the incoming H_2 molecule are described both in atomic coordinates (x_a/x_b, y_a/y_b, z_a/z_b) and molecular, center-of-mass (CoM) coordinates (X, Y, Z), with the H–H distance r_{H-H}, the polar angle θ, and the azimuthal angle ϕ relative to the x axis. The surface atoms are described using only atomic coordinates (x_l, y_l, z_l).

our incoming D_2 and its interaction with the surface, while the forces between the copper atoms are described by the EAM. Newton's third law can be applied then to also find the effect of the incoming D_2 of the surface Cu atoms. We will refer to this method as the dynamic corrugation model (DCM) using the EAM potential (EAM-DCM).

With these initial conditions defined, we propagate our molecule (and surface) according to Hamilton's equations of motion using the simple Hamiltonian

$$H = \sum_{i=0}^{n}\left[\frac{p_i^2}{2m_i}\right] + V(R(t)), \tag{13}$$

where p_i and m_i are, respectively, the momentum and mass of the ith atom. $V(R(t))$ describes the total potential energy of all n atoms at positions R and time t. The Bulirsch–Stoer predictor-corrector algorithm is used for propagation because of its accuracy and relative speed.[56] For reactive trajectories, propagation ends when the two deuterium atoms are separated more than 2.25 Å from each other within the maximum propagation time frame of 20 ps. Those molecules that are reflected and move away further than the initial starting distance of 7 Å from the surface in the Z-coordinate are considered scattered. These molecules are binned to a final rovibrational state and separated into elastically scattered atoms, for those in the same state as the initial rovibrational state, or in-elastically, for those that return in a different rovibrational state. Binning is performed by first finding the closest allowed ($\Delta J = \pm 2$) rotational state using the classical angular energy and then finding the closest vibrational state in energy to this rotational state.

Finally, those molecules that neither scatter nor react within the maximum time interval of 20 ps are considered trapped on the surface. Only for very low incidence energies were these found in significant quantities, primarily due to the very low velocity of the D_2 toward the surface, and thus, they did not significantly contribute to the final reaction and scattering probabilities found in this work. Results were obtained for ~100.000 trajectories when using a static surface, compared to at least 4.000 trajectories of EAM-DCM, at a modeled surface temperature of 925 K.

Reaction probabilities and rovibrational (in)elastic scattering probabilities are obtained by dividing the number of reacted or (in)elasticly scattered trajectories by the total amount of trajectories computed at each normal incidence energy.

D. SCM slab generation

To model thermally distorted copper surfaces, slabs of Cu(111) surfaces are generated. Previous work with the SCM achieved this using random displacements of each individual atom from its ideal lattice position. Here, the displacement was assumed to be both bulk-like and uniform in the three Cartesian directions. The magnitude of this displacement is randomly selected from a Gaussian distribution with a standard deviation of

$$\sigma = \sqrt{\frac{3B}{8\pi^2}}. \tag{14}$$

Here, B is the temperature dependent Debye–Waller factor obtained from fits to experimental inelastic neutron scattering data.[57]

With this random displacement in place, the surface slab positions are next expanded along the u and v lattice coordinates based on an experimental thermal expansion coefficient.[54] Furthermore, the interlayer distances, found in the z-direction of the slab, are taken directly from experimental results.[55] This approach to surface slab generation we will refer to as random displacement SCM (RD-SCM) and is what has been used in all previous works of the SCM.

To validate this methodology, surface slabs were also generated using the EAM potential published by Sheng *et al.*[36] A cell of 7 × 7 × 7 Cu atoms was modeled first in a bulk environment by applying a minimum image convention in all three Cartesian directions. These atoms are then relaxed based on the modeled temperature using a Berendsen thermostat.[58] Then, three of the lowest atom layers, for a total of 147 atoms, were kept frozen, while a vacuum is introduced on the other side of the slab. This slab is then again relaxed, now as a surface. Positions and momenta of each slab atom are then recorded and collected to be used while running surface dynamics calculations. Further computational details can be found in the Appendix. Thus, the slab is generated without any external scaling based on different experimental results, as was done in the RD-SCM approach. It is important to note that an EAM potential is not the only pathway to obtaining such a surface slab, as other potentials could also be implemented.

In this work, we will refer to dynamics on such an EAM surface as EAM-SCM if the surface atoms are not included into the dynamics in contrast to the EAM-DCM approach, where the surface atoms are explicitly included into the dynamics. Both methods, the SCM and the DCM, use the basis of Eq. (1): the V_{CRP} BOSS PES as V_{DFT} (ideal) and the expression of Eq. (3) as V_{coup}. The EAM is used to model V_{strain} of Eq. (1) and is only explicitly needed in the dynamics for EAM-DCM. Furthermore, it is used to generate static surface slabs for the EAM-SCM approach.

E. Simulating time-of-flight spectra

To better compare to experimental data, the results from our dissociation simulations were fitted to obtain functional forms matching those of time-of-flight (ToF) spectra.

This was done using a two-step process: first, our theoretical results are fitted to a functional form matching a reaction probability curve to obtain the width parameter, saturation parameter, and effective barrier height. Next, we combine this fit with several parameters, including some geometrical constraints, of the experimental setup of Auerbach *et al.*[8] to simulate ToF spectra for our different QCT approaches.

This fitting procedure, as well as the functional form used for the reaction probability, and the generalized logistic function (LGS) were obtained from earlier work by Nattino *et al.*,[15]

$$S(E) = \frac{A}{\left(1 + \nu \exp\left[-\frac{E-E_0'}{W'}\right]\right)^{\frac{1}{\nu}}}. \tag{15}$$

Here, A is the saturation parameter, which controls the maximum value of the ToF curve, E_0 is the effective barrier parameter, and W is the width parameter. With the ν parameter, the shape of the curve can be further adjusted to a number of related functional forms, such as an ordinary logistic function ($\nu = 1$) and the Gompertz function ($\nu \to 0^+$).

III. RESULTS AND DISCUSSION

A. Reaction probability curves

To validate the quality and physical relevance of the random displacement approach to generating SCM surface slabs (RD-SCM), we will compare the dissociative chemisorption reaction probabilities obtained with this approach to those obtained using surface slabs generated with an EAM potential (EAM-SCM). Also included are dissociation curves for the same dynamics on a moving surface using the EAM potential to also describe the interactions between the copper atoms. We will refer to this method as the dynamic corrugation model (DCM) using an EAM potential (EAM-DCM). Comparisons between these different methods will give us insight not only into the quality of the RD-SCM generated surface slabs but also into the effect of energy exchange with our moving surface and the validity of the sudden approach as we use it in the SCM models. Finally, we include the results of an ideal, 0 K static surface, which we obtain using the often used BOSS approach to look at the general effect the different models for including surface temperature effects have on the dissociation curves.

In Fig. 2, we show the reaction probability curves for several different rovibrational states. As expected, the general trend for all the different approaches is relatively similar. At low incidence energy, the D_2 molecule does not have enough energy to pass over the minimum energy barrier for dissociation, and reaction probability will be minimal. As the normal incidence energy increases so does dissociation probability, until it reaches a maximum, or saturation, value.

The first point of note in this figure is the difference in saturation values between the different approaches. Both the RD-SCM and BOSS methods show a similar saturation at around 0.9, while the EAM-SCM and EAM-DCM approaches both have a lower value at around 0.85, with the EAM-DCM approach always being slightly higher. This could indicate that the surface slabs generated with the EAM potential contain somewhat higher maximum barriers compared to those generated through the RD-SCM. These values are, however, very difficult to obtain experimentally and thus is of much less importance for the quality of our model when comparing to experiment.[15]

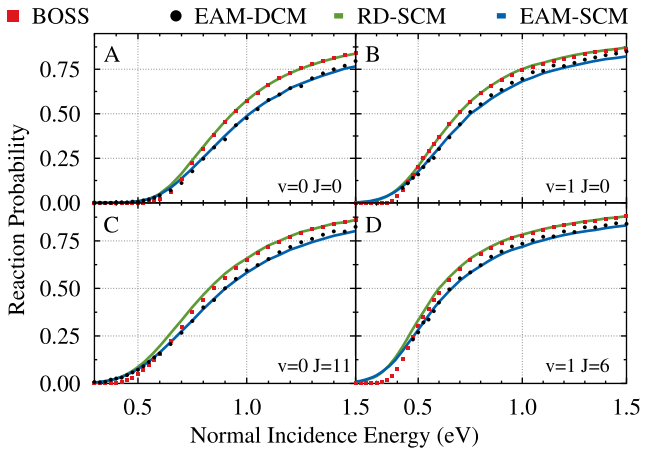

FIG. 2. State-specific reaction probabilities for the D_2 on Cu(111) system and for four different approaches: BOSS (red squares), RD-SCM (green curve), EAM-SCM (blue curve), and EAM-DCM (black circles). For the CM approaches, a modeled surface temperature of 925 K was used. Shown are the initial rovibrational states (a) v = 0, J = 0; (b) v = 1, J = 0; (c) v = 0 J = 11; (d) v = 1, J = 6.

All three CM approaches (RD-SCM, EAM-SCM, and EAM-DCM) predict a higher reaction probability than that shown by the BOSS model, yet their curves do not increase as steeply. This broadening of the S-curve is generally attributed to surface temperature effects and has been extensively discussed in earlier work.[22,23,59] Both the EAM-SCM and EAM-DCM show a bit more broadening than the RD-SCM approach, although it is harder to quantize due to the lower saturation value. This is especially of note as previous work has shown some indication that the width and the saturation value of the dissociation curves are not completely independent.[22]

The availability of energy exchange appears to only very limitedly affect our system, as we find great agreement between the static surface approach of the EAM-SCM and the dynamic surface approach of the EAM-DCM. Although earlier work has shown similar results for H_2,[16,60–62] this is one of the first examples of a direct and extensive comparison between almost identical methods, one with a dynamic surface and one without.

B. (In)elastic scattering probabilities

To further analyze our dissociation simulations, we can also look at the rovibrational elastic and inelastic scattering probabilities. In Fig. 3, we again compare the BOSS (red squares), RD-SCM (green curves), EAM-SCM (blue curves), and EAM-DCM (black circles) methods, now for the elastic [(b), (d), (f), and (h)] and in-elastic [(a), (c), (e), and (f)] rovibrational scattering probabilities for the same initial states as discussed before.

In general, we find a preference for elastic scattering at lower incidence energies, where there is no enough energy available within the molecule to reach other rovibrational states. As the kinetic energy of the molecule increases, more and more rovibrational states become available and we find higher and higher probability for inelastic scattering. At very high incidence energies, chemisorption dominates and only limited scattering is observed.

For the rovibrational ground state [(a) and (b)], as well as the vibrationally excited states [(c), (d), (g), and (h)], the BOSS model predicts much higher elastic scattering for the lower incidence energies. Moving to higher energies, we again see almost perfect agreement with the RD-SCM curves and qualitative agreement with the EAM-SCM and EAM-DCM approaches. Surprisingly, this effect is absent for the v = 0, J = 11 state, where the BOSS model shows good agreement with the all CM results for all incidence energies.

Agreement between the EAM-SCM and EAM-DCM approaches is again very good, with only minor differences that we can partially attribute to the relatively low amount of trajectories run for the EAM-DCM approach. This further validates the quality of the SCM sudden approach. As the main difference between these two approaches is the possibility of energy exchange between the copper surface and the D_2 molecule, this agreement further enforces our observation of the limited effect of energy exchange on not only the final dissociation results but also on these rovibrational (in)elastic scattering results. The latter are expected to be more sensitive to

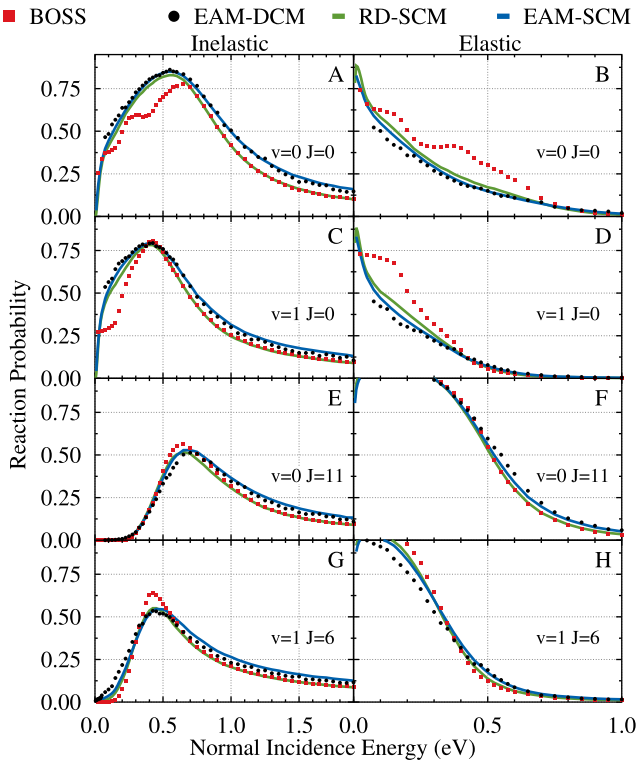

FIG. 3. State-specific, elastic [(b), (d), (f), and (h)], and inelastic [(a), (c), (e), and (g)] scattering probabilities for the D_2 on Cu(111) system and for four different approaches: BOSS (red squares), RD-SCM (green curves), EAM-SCM (blue curves), and EAM-DCM (black circles). For the CM approaches, a modeled surface temperature of 925 K was used. Shown are the initial rovibrational states: [(a) and (b)] v = 0, J = 0; [(c) and (d)] v = 1, J = 0; [(e) and (f)] v = 0 J = 11; [(g) and (h)] v = 1, J = 6.

details of the PES and the exchange of energy between D_2 and the surface.

Interestingly, an analysis of the energy exchange in our DCM trajectories does show a small transfer of energy between the copper surface and the D_2 molecule. At very low incidence energies (<150 meV), we primarily find a flow of energy into the D_2 (<10%), while at higher incidence energies, we primarily find a drain of energy into the surface (≈15%). This drain of energy was found to be predominantly flowing from the translational energy of the D_2 molecule. Consequently, little difference was found in the rovibrational energy of scattered molecules when comparing the EAM-DCM and EAM-SCM approaches. Furthermore, the average turning point of the scattered molecules was found to be similar between these two methods. This, combined with the minimal differences in (in)elastic rovibrational scattering probabilities, leads us to believe that this energy exchange, as a result of a mostly mechanical coupling, primarily occurs after the scattering event, as the D_2 moves away from the surface. We are not aware of any previous works discussing this phenomenon without there being additional particles already on the surface[63] and as such would consider it of great interest for future work.

The energy exchange at very low incidence energies does appear to affect the final rovibrational state of the scattered molecules and appears to be directly related to the z-coordinate as molecules that get closer to the surface obtain a larger amount of energy. It remains however a question on how accurate the QCT method is for these very low incidence energies and to what extent quantum dynamical effects, such as zero point energy conservation, of the molecule and the surface atoms play a role.[2]

C. Simulated time-of-flight spectra

To better compare our theoretical results to experiment, our reaction probability curves were used to simulate time-of-flight (ToF) spectra following the procedure as outlined by Nattino *et al.*[15] As experimental results are often obtained in the form of ToF spectra and are generally most sensitive for the curve onset of the initial state specific reaction probability curve, we believe that ToF spectra are one of the better ways of comparing theoretical results to experimental data, especially when correct and accurate experimental ToF parameters are known and have been published. Thus, this work is of great interest as it both simulated ToF spectra and fit experimental results using the same expression.

Simulated spectra of a selection of four different rovibrational states for the four theoretical approaches discussed in this work are shown in Fig. 4. The rovibrational states shown were chosen such that they cover a variety of different excited states, as well as the rovibrational ground state. Furthermore, we also included the experimental results from Auerbach *et al.*[8] refit in earlier work, as well as AIMD results, both obtained from the work by Nattino *et al.*[15] These experimental results were obtained from recombinative desorption experiments of D_2 permeating through the bulk metal to a Cu(111) surface at a surface temperature of 925 K and as such rely on the applicability of detailed balance.[8] Surface motion effects were included in these AIMD results, applying a modeled surface temperature of 925 K.

Figures 4(a), 4(e), and 4(i) show our simulated results for the rovibrational ground state. Good agreement between the different CM approaches is found, as was the case for the chemical desorption curves. A slight difference between peak width is observable, with the EAM-SCM approach showing the highest width. The peak location, however, appears to be the same for all three methods. The BOSS model, on the other hand, shows a much more narrow peak with a peak location at a shorter time of flight. The AIMD peak can be found at approximately the same value as the CM peaks, yet its width is significantly lower. In contrast, looking at the experimental curve, we observe a width similar to that of the CM approaches. The curve is, however, shifted compared to the CM curves, showing a peak location at a higher time of flight.

A similar thing can be observed in Figs. 4(b), 4(f), and 4(j) for the vibrationally excited v = 1, J = 0 state. Unfortunately, however, no AIMD data were available for this state. The width for the three CM approaches is once again similar and close to that of the experimental results. Peak location also shows similar results, with the CM approaches underestimating that of the experiment. The BOSS model shows the worst agreement, with a much narrower peak and a peak height about twice as far from experiment.

Moving to the rotationally excited states in Figs. 4(e)–4(h), we again see that the BOSS model yields both the narrowest peak, as well

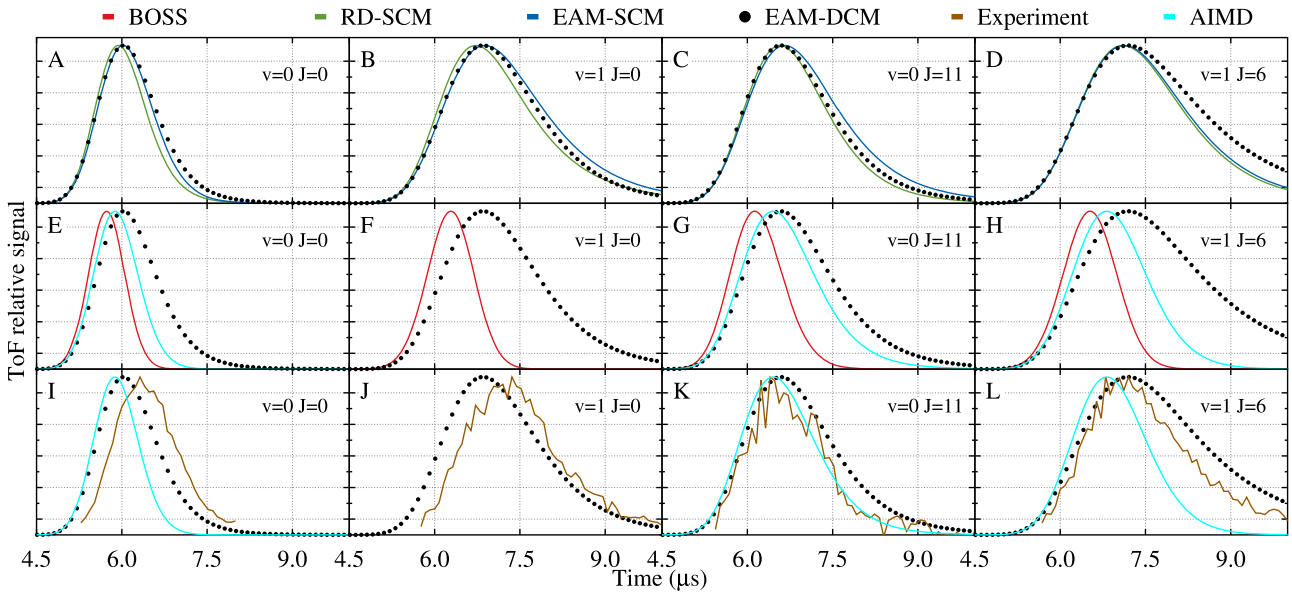

FIG. 4. Simulated time-of-flight spectra for the D_2 on Cu(111) system. For four different rovibrational states, RD-SCM (green curves), EAM-SCM (blue curves), and EAM-DCM (black circles) are compared to each other [(a)–(d)], as well as to the BOSS approach (red curves) [(e)–(h)], and refitted experimental results (orange curves) [(i)–(l)] and AIMD results (cyan curves) [(e)–(l)] from Nattino *et al.*[15] For the CM approaches and the AIMD results, a modeled surface temperature of 925 K was used, which matches the conditions of the experiment. Shown are the initial rovibrational states: [(a), (e), and (i)] v = 0, J = 0; [(b), (f), and (j)] v = 1, J = 0; [(c), (g), and (k)] v = 0 J = 11; [(d), (h), and (l)] v = 1, J = 6.

as the lower time of flight for the peak. The different CM approaches show peaks at the highest time of flight, each with approximately the same value. The experimental results are found somewhere between these peaks, with a width closer to that of the CM results. AIMD results for these curves are a bit mixed as the agreement for the v = 0, J = 11 state appears to be almost perfect, while agreement with the v = 1, J = 6 experimental data is much worse.

Overall, we see improved agreement with experiment when including the SCM and DCM approaches, regardless of which variation.

RD-SCM, EAM-SCM, and EAM-DCM all show very similar results, with RD-SCM always showing the narrowest peak of the three. Due to the nature of simulating the time-of-flight spectra, however, small variations are expected. The results when using the BOSS model showed the narrowest peaks as well as the shortest time-of-flight for each rovibrational state we investigated, often well below the value found in experiment. This matches findings from earlier work.[15]

D. Effect of RD-SCM on atom displacement

In an attempt to directly compare the randomly generated and EAM generated surface slabs, we investigated the displacements of each individual surface slab atom for every Cartesian coordinate. Only those atoms within the SCM cutoff distance of 16 bohrs were included in these results. As was discussed in Sec. II, the RD-SCM approach makes use of the Debye–Waller factor to calculate the standard deviation for the Gaussian displacement of each surface atom. The EAM-SCM approach instead uses surface slabs simulated through another potential, in our case the EAM. Assuming the simulation attains a proper thermodynamic equilibrium, this approach should also result in a Gaussian distribution for our displacements.

In Fig. 5, we outlined the displacements in the x- [(a) and (c)] and y-direction [(b) and (d)] both at the onset of the reaction probability curve [(a) and (b)] and at the saturation value [(c) and (d)]. Only those surface slab atoms at the top layer were included in these results. Separate curves were also included for only those trajectories where the D_2 dissociated.

Comparing the RD-SCM displacements for all trajectories (red) to only those that reacted (green), we see very similar curves both for the x- and y-coordinates. Due to the low reaction probability at the curve onset, the dataset for the reacted trajectories shows a decent amount of noise. This is significantly decreased when looking at the saturation value, although there is still a significant variation in results for very low displacements. There also appears to be a slight preference toward a positive displacement. It is unclear yet why this occurs.

Similar noise is found with the EAM-SCM results for the reacted trajectories at low incidence energy. This, however, disappears when moving toward high energy or also when including the trajectories that did not react. Furthermore, no clear preference can be found toward a positive or negative displacement, as would be expected for in-plane displacements.

Comparing the two methods to each other, we do see a clear difference. While both approaches appear to result in a normal distribution of displacements, they do have a very different width, with the EAM-SCM displacements, obtained from EAM surface slab simulations, showing much broader peaks.

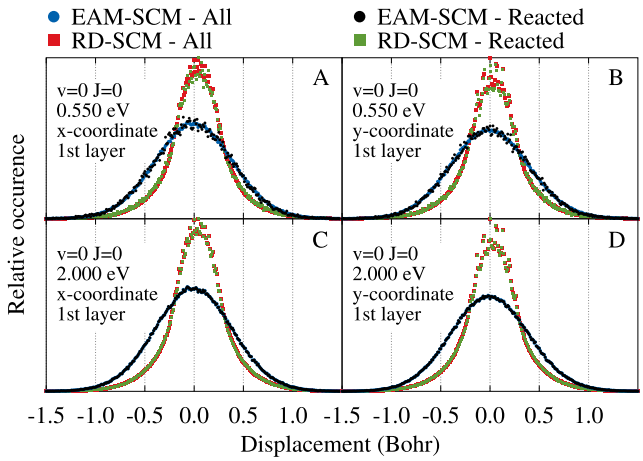

FIG. 5. Surface slab atom displacement at a modeled surface temperature of 925 K relative to the ideal, 0 K lattice. Only those atoms in the first surface layer are included for those trajectories run on the rovibrational ground state. Included are the displacements both for those trajectories that reacted and for all trajectories run for RD-SCM, green and red squares, respectively, and EAM-SCM, black and blue circles, respectively. Displacements are shown for D_2 normal incidence energies of 0.550 eV [(a) and (b)] or 2.000 eV [(c) and (d)], separating the x-coordinate [(a) and (c)] and y-coordinate [(b) and (d)].

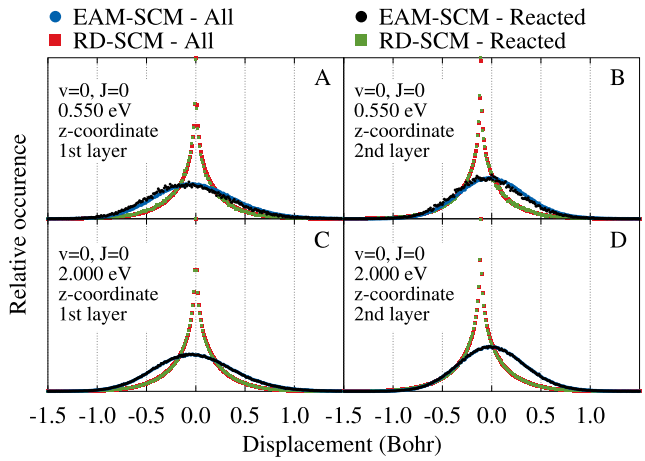

FIG. 6. Surface slab atom displacement at a modeled surface temperature of 925 K relative to the ideal, 0 K lattice. Only those trajectories run on the rovibrational ground state are shown. Included are the displacements both for those trajectories that reacted and for all trajectories run for RD-SCM, green and red squares, respectively, and EAM-SCM, black and blue circles, respectively. Displacements are shown for D_2 normal incidence energies of 0.550 eV [(a) and (b)] or 2.000 eV [(c) and (d)] both for the first surface slab layer [(a) and (c)] and the second layer [(b) and (d)].

Next, we discuss the most interesting of the three Cartesian directions, the z-coordinate. Displacements toward (+z), or away from (−z), the incoming reactant molecules have in previous works been shown to affect dissociation probabilities.[27,28,64,65] For example, Bonfanti *et al.* used a simple 7D model to quantum dynamically show increased reaction probabilities when surface layer atoms are moved away from the incoming H_2 molecule.[64]

In Figs. 6(a) and 6(b), we compare the EAM-SCM and RD-SCM results at the reaction probability curve onset for the first and second surface layer atoms. Again only those trajectories that reacted were included separately. For EAM-SCM, reacted trajectories appear to show a clear preference toward a negative displacement in z, away from the D_2 molecule, as the peak of the atom displacement distribution is slightly shifted toward negative z. This phenomenon can be observed both for the first layer (a) and the second layer (b) and matches the results found with the simple 7D model.[64] Interestingly, the opposite effect is found for the CH_4 on Pt(111), Ir(111), and Ni(111) systems, where surface atom displacement away from the reactant increased the barrier height.[27,28,65] Furthermore, limited surface puckering out of the surface is expected when treating this system dynamically as systems with a large mass mismatch have been shown to be primarily dominated by the recoil effect.[27,28]

A similar effect cannot be seen with the results for the RD-SCM approach as both the reacted and total slab distributions show a similar width and peak location. This distribution also does not appear to be that of a Gaussian. We attribute this to the way the displacements are generated as it is only ensured that the total displacements in the direction of the displacement, and not x, y, or z individually, follow a Gaussian distribution with the standard deviation calculated with the Debye–Waller factor. Similar distributions are thus found when looking along the u- and v-axes for the (111) surface slab. Furthermore, the second layer shows a static shift of negative z. This is also attributed to the RD surface slab generation, as experimental interlayer distances are applied when generating the surface, instead of the bulk lattice constant, as is used for the x- and y-directions.

At much higher incidence energies [(c) and (d)], we no longer see the EAM-SCM preference toward a negative z-displacement. At such a high energy, almost all trajectories will react, making the lowest barrier path much less visible. For the RD-SCM results, we again see this second layer shift due to the experimental interlayer distance.

IV. CONCLUSION

Using the dissociation of D_2 on Cu(111) as a model system, we investigated the physical relevance of the random displacement approach to SCM surface slab generation.[22,23] Surface slabs were generated using both this approach and a highly accurate EAM potential, which has been shown to accurately describe copper bulk and surfaces.[36] Furthermore, we used this EAM potential to dynamically treat our surface, allowing us to both test the validity of the sudden approach and investigate any effect of energy exchange with the surface, which has long been theorized to be of little importance for this system.[23] Each calculation used the same CRP PES based on the SRP48 functional as had been used in previous works, with the SCM approaches all applying the effective 3-body potential as published by Spiering *et al.*[23]

We found good agreement between the dissociation curves of the RD-SCM and the EAM-SCM approaches, as well as with the

EAM-DCM approach. Agreement was especially good for the reaction curve onset, which has been shown to be the most accurate for experimental results, while the saturation value was found to be lower for the two methods based on the EAM surface slabs. All three methods resulted in increased broadening of the dissociation S-curve compared to the BOSS approach, which is generally attributed to surface temperature effects.

Similar agreement was found for rovibrational (in)elastic scattering curves, where only the BOSS model significantly deviated from the results found with the different CM approaches. The good agreement between EAM-SCM and EAM-DCM indicated limited to no effect of energy exchange on the reaction and, more importantly, the (in)elastic scattering probabilities, although we did find a drain of 15% of the translational energy of the scattered molecules for almost the entire incidence energy range, which we have not found to be reported in other works.

A further evaluation of the dissociation curves was performed by simulating a time-of-flight spectrum for each curve fitted to a standard form. Such a simulated spectrum is especially sensitive to the reaction curve onset, as had been seen in earlier work. Again, we found great agreement between the different CM approaches, as well as improved agreement with experiment[15] compared to the BOSS method.

To directly compare the surface slabs generated for the RD-SCM and EAM-SCM approaches, we mapped the displacements for each individual surface atom from its ideal lattice position both for all trajectories and for only those that reacted. As expected, no preference was found for either method when considering the x- and y-coordinate, although the EAM generated slabs did show a much broader distribution of displacements. For the z-coordinate, however, we found a clear preference for reaction when the surface atoms are displaced away from the incoming D_2 but only for the EAM-SCM approach. Surface slabs generated using the RD-SCM did not even show Guassian distributions in their displacement as the displacement method only ensured a normal distribution in the total displacement of the atom.

In general, we found good agreement between the reaction probabilities and rovibrational (in)elastic scattering probabilities obtained using the EAM-SCM and RD-SCM approaches, although the RD-SCM approach to surface generation showed much narrower atom displacement distributions. Furthermore, the good agreement with the non-static surface approach of EAM-DCM indicated both the very limited effect of energy exchange on the dissociation and (in)elastic scattering probabilities, despite having observed some energy drain into the surface.

With the success of the SCM sudden approach, combined with physically relevant surfaces generated with an EAM potential, we have opened a pathway toward quantum dynamically treating the motion of D_2 on a non-ideal Cu(111) surface. Accurate quantum dynamical treatment of such systems would be a major step forward in describing the rovibrational (in)elastic scattering as well as the low incidence energy regime, which are dominated by quantum effects ill-described by QCT dynamics.

ACKNOWLEDGMENTS

The authors would like to thank Dr. Paul Spiering and Robert van Bree for helpful insights and useful discussion.

APPENDIX: ADDITIONAL COMPUTATIONAL DETAILS

In this work, we used the highly accurate EAM potential for copper as described by Sheng *et al.*[36] The 1001 equidistant data points of the pair, density, and embedding functions were fitted using cubic splines, with a cutoff at 0 Å and 6.5 Å for the pair and density function and a cutoff at 0.0 and 1.0 density for the embedding function. Outside these final spline knots, both the value and derivative of the functions yield 0.

NVT dynamics were run using a velocity-Verlet algorithm[66] and the Berendsen thermostat,[58] while NVE propagation was performed using the Bulirsch–Stoer predictor-corrector algorithm.[19]

Stepwise volume scaling was performed to equilibrate the pressure and Cu lattice constant by running 1 ps of NVT dynamics and storing the virial pressure each step using the equation[67]

$$P_{vir} = Nk_bT + \frac{1}{2} \times \frac{1}{3} \sum_{i \neq j} r_{ij} \cdot F_{ij}, \tag{A1}$$

where N is the number of (mobile) surface atoms, k_b is the Boltzmann constant, T is the instantaneous surface temperature, and r_{ij} and F_{ij} are, respectively, the distance and force between surface atoms i and j. Due to double counting, this dot product in halved. The total average pressure is then divided by a scaling factor of 2500 GPa and used to scale the simulation box volume. This scaling factor was chosen arbitrarily to ensure the surface is not scaled too fast or too slow.

To ensure this yields satisfactory results, we also determine the pressure from the diagonal components of the virial stress tensor. Both these methods are grounded in theory and will result in the same values under equilibrated conditions.[67]

1. Bulk lattice constant determination

To determine our relaxed bulk lattice constant, a cell of $7 \times 7 \times 7$ Cu atoms was placed in the optimal FCC lattice structure. Some initial momentum was also included using a normal distribution based on the modeled surface temperature. This is to avoid any rapid changes during the initial surface relaxation steps. The minimum image convention is applied in the x, y, and z Cartesian directions. Next, this slab was propagated in the canonical ensemble (NVT) for 40 000 steps with a step size of 0.005 ps, yielding a total propagation of 200 ps. Volume rescaling was performed between 40 ps and 160 ps of this run, scaling every ps to ensure the thermodynamically favored box volume is attained. To evaluate the quality of this run, the average atom–atom distance, temperature, and kinetic and potential energy of the bulk copper are calculated each step and stored for evaluation. Next, this NVT relaxed bulk is propagated for 250 steps (≈6 ps) in the micro-canonical ensemble (NVE), where total propagation time varies due to the use of a predictor-corrector algorithm. Here, we again evaluate the stability of our copper based on the temperature, average atom–atom distance, kinetic and potential energies, and virial pressure and virial stress. The relaxed bulk lattice constant is finally obtained from the final volume of our box. This is repeated 200 times, each with a unique seed to generate the initial conditions, to obtain the average bulk lattice constant of this potential for our chosen temperature.

2. Surface slab generation

To generate surface slabs, we take our bulk lattice constant to generate the initial $7 \times 7 \times 7$ FCC copper lattice and again apply some

initial momentum from a normal distribution based on the modeled surface temperature. We further repeat all steps for our bulk lattice, as described above, but without applying any volume rescaling.

Then, three consecutive outer layers of our surface slab, for a total of 147 atoms, are set locked to their current positions, and the minimum image convention is applied only in the x- and y-directions. This new surface slab is then propagated in the canonical ensemble for a total of 250 ps and a step size of 0.0005 ps (50 000 steps). It is important to note that we do not apply any volume rescaling during these steps to ensure our static layers properly model the bulk. This does also mean that our top layers will exhibit some stress due to the change in pressure when moving from bulk to a surface. A short NVE run of 1000 steps (≈40 ps) is again used to determine the stability of our surface slab. To ensure the surface slab atoms are always located approximately at the same position, we next attempt to recenter our slab. We then performed an NVE dynamics run of 25 000 steps (≈1100 ps), logging the average position of each atom in the top layer of our surface slab. After this run, we shift our entire slab, including the static, bulk-like, layers, so that the average position of the entire top layer is found at (x, y, z) = (0, 0, 0). With this process completed, we start our final dynamics run to obtain traces of our surface slab positions and momenta. During an NVE dynamics run of 1250 steps, we take a snapshot every 50 steps (≈2 ps) of both the surface slab positions and momenta for a total of 25 snapshots each. To obtain a suitable and diverse amount of traces, we repeat this entire surface slab generation scheme 1000 times for a total of 25 000 surface slab positions with matching momenta. These can then be loaded into our SCM dynamics as an alternative to the random displacement approach of the earlier works.

DATA AVAILABILITY

The data that support the findings of this study are available from the research group's public repository at https://pubs.tc.lic.leidenuniv.nl/.

REFERENCES

[1] A. C. Luntz, "The dynamics of making and breaking bonds at surfaces," in *Chemical Bonding at Surfaces and Interfaces*, edited by A. Nilsson, L. G. M. Pettersson, and J. K. Nørskov (Elsevier, Amsterdam, 2008), Chap. 3, pp. 143–254.

[2] G.-J. Kroes and M. F. Somers, "Six-dimensional dynamics of dissociative chemisorption of H_2 on metal surfaces," J. Theor. Comput. Chem. **04**, 493–581 (2005).

[3] G.-J. Kroes and C. Díaz, "Quantum and classical dynamics of reactive scattering of H_2 from metal surfaces," Chem. Soc. Rev. **45**, 3658–3700 (2016).

[4] C. Smith, A. K. Hill, and L. Torrente-Murciano, "Current and future role of Haber–Bosch ammonia in a carbon-free energy landscape," Energy Environ. Sci. **13**, 331–344 (2020).

[5] T. Zambelli, J. V. Barth, J. Wintterlin, and G. Ertl, "Complex pathways in dissociative adsorption of oxygen on platinum," Nature **390**(6659), 495–497 (1997).

[6] G. Anger, A. Winkler, and K. D. Rendulic, "Adsorption and desorption kinetics in the systems H_2/Cu(111), H_2/Cu(110), and H_2/Cu(100)," Surf. Sci. **220**, 1–17 (1989).

[7] H. Hou, S. J. Gulding, C. T. Rettner, A. M. Wodtke, and D. J. Auerbach, "The stereodynamics of a gas-surface reaction," Science **277**, 80–82 (1997).

[8] H. A. Michelsen, C. T. Rettner, D. J. Auerbach, and R. N. Zare, "Effect of rotation on the translational and vibrational energy dependence of the dissociative adsorption of D_2 on Cu(111)," J. Chem. Phys. **98**, 8294–8307 (1993).

[9] C. T. Rettner, H. A. Michelsen, and D. J. Auerbach, "Quantum-state-specific dynamics of the dissociative adsorption and associative desorption of H_2 at a Cu(111) surface," J. Chem. Phys. **102**, 4625–4641 (1995).

[10] Rotational excitation and vibrational relaxation of H_2 scattered from Cu(111).

[11] H. A. Michelsen and D. J. Auerbach, "A critical examination of data on the dissociative adsorption and associative desorption of hydrogen at copper surfaces," J. Chem. Phys. **94**, 7502–7520 (1991).

[12] K. Cao, G. Füchsel, A. W. Kleyn, and L. B. F. Juurlink, "Hydrogen adsorption and desorption from Cu(111) and Cu(211)," Phys. Chem. Chem. Phys. **20**, 22477–22488 (2018).

[13] C. Díaz, E. Pijper, R. A. Olsen, H. F. Busnengo, D. J. Auerbach, and G. J. Kroes, "Chemically accurate simulation of a prototypical surface reaction: H_2 dissociation on Cu(111)," Science **326**, 832–834 (2009).

[14] A. Mondal, M. Wijzenbroek, M. Bonfanti, C. Díaz, and G.-J. Kroes, "Thermal lattice expansion effect on reactive scattering of H_2 from Cu(111) at Ts = 925 K," J. Phys. Chem. A **117**, 8770–8781 (2013).

[15] F. Nattino, A. Genova, M. Guijt, A. S. Muzas, C. Díaz, D. J. Auerbach, and G.-J. Kroes, "Dissociation and recombination of D_2 on Cu(111): *Ab initio* molecular dynamics calculations and improved analysis of desorption experiments," J. Chem. Phys. **141**, 124705 (2014).

[16] F. Nattino, C. Díaz, B. Jackson, and G.-J. Kroes, "Effect of surface motion on the rotational quadrupole alignment parameter of D_2 reacting on Cu(111)," Phys. Rev. Lett. **108**, 236104 (2012).

[17] E. W. F. Smeets, J. Voss, and G.-J. Kroes, "Specific reaction parameter density functional based on the meta-generalized gradient approximation: Application to H_2 + Cu(111) and H_2 + Ag(111)," J. Phys. Chem. A **123**, 5395–5406 (2019).

[18] M. Wijzenbroek, D. M. Klein, B. Smits, M. F. Somers, and G.-J. Kroes, "Performance of a non-local van der Waals density functional on the dissociation of H_2 on metal surfaces," J. Phys. Chem. A **119**, 12146–12158 (2015).

[19] H. F. Busnengo, A. Salin, and W. Dong, "Representation of the 6D potential energy surface for a diatomic molecule near a solid surface," J. Chem. Phys. **112**, 7641–7651 (2000).

[20] C. Díaz, R. A. Olsen, D. J. Auerbach, and G. J. Kroes, "Six-dimensional dynamics study of reactive and non reactive scattering of H_2 from Cu(111) using a chemically accurate potential energy surface," Phys. Chem. Chem. Phys. **12**, 6499–6519 (2010).

[21] G.-J. Kroes, C. Díaz, E. Pijper, R. A. Olsen, and D. J. Auerbach, "Apparent failure of the Born–Oppenheimer static surface model for vibrational excitation of molecular hydrogen on copper," Proc. Natl. Acad. Sci. U. S. A. **107**, 20881–20886 (2010).

[22] M. Wijzenbroek and M. F. Somers, "Static surface temperature effects on the dissociation of H_2 and D_2 on Cu(111)," J. Chem. Phys. **137**, 054703 (2012).

[23] P. Spiering, M. Wijzenbroek, and M. F. Somers, "An improved static corrugation model," J. Chem. Phys. **149**, 234702 (2018).

[24] Y. Xiao, W. Dong, and H. F. Busnengo, "Reactive force fields for surface chemical reactions: A case study with hydrogen dissociation on Pd surfaces," J. Chem. Phys. **132**, 014704 (2010).

[25] G. N. Seminara, I. F. Peludhero, W. Dong, A. E. Martínez, and H. F. Busnengo, "Molecular dynamics study of molecular and dissociative adsorption using system-specific force fields based on *ab initio* calculations: CO/Cu(110) and CH_4/Pt(110)," Top. Catal. **62**, 1044–1052 (2019).

[26] A. Lozano, X. J. Shen, R. Moiraghi, W. Dong, and H. F. Busnengo, "Cutting a chemical bond with demon's scissors: Mode- and bond-selective reactivity of methane on metal surfaces," Surf. Sci. React. Concepts Surf.: Coupling Theory Exp. **640**, 25–35 (2015).

[27] A. K. Tiwari, S. Nave, and B. Jackson, "Methane dissociation on Ni(111): A new understanding of the lattice effect," Phys. Rev. Lett. **103**, 253201 (2009).

[28] S. Nave and B. Jackson, "Methane dissociation on Ni(111) and Pt(111): Energetic and dynamical studies," J. Chem. Phys. **130**, 054701 (2009).

[29] A. K. Tiwari, S. Nave, and B. Jackson, "The temperature dependence of methane dissociation on Ni(111) and Pt(111): Mixed quantum-classical studies of the lattice response," J. Chem. Phys. **132**, 134702 (2010).

[30] D. Han, S. Nave, and B. Jackson, "Dissociative chemisorption of methane on Pt(110)-(12): Effects of lattice motion on reactions at step edges," J. Phys. Chem. A **117**, 8651–8659 (2013).

[31]H. Guo, A. Farjamnia, and B. Jackson, "Effects of lattice motion on dissociative chemisorption: Toward a rigorous comparison of theory with molecular beam experiments," J. Phys. Chem. Lett. **7**, 4576–4584 (2016).
[32]G. J. Kroes, M. Wijzenbroek, and J. R. Manson, "Possible effect of static surface disorder on diffractive scattering of H_2 from Ru(0001): Comparison between theory and experiment," J. Chem. Phys. **147**, 244705 (2017).
[33]N. Artrith and J. Behler, "High-dimensional neural network potentials for metal surfaces: A prototype study for copper," Phys. Rev. B **85**, 045439 (2012).
[34]J. Behler and M. Parrinello, "Generalized neural-network representation of high-dimensional potential-energy surfaces," Phys. Rev. Lett. **98**, 146401 (2007).
[35]J. Behler, "First principles neural network potentials for reactive simulations of large molecular and condensed systems," Angew. Chem., Int. Ed. **56**, 12828–12840 (2017).
[36]H. W. Sheng, M. J. Kramer, A. Cadien, T. Fujita, and M. W. Chen, "Highly optimized embedded-atom-method potentials for fourteen fcc metals," Phys. Rev. B **83**, 134118 (2011).
[37]G. Füchsel, K. Cao, S. Er, E. W. F. Smeets, A. W. Kleyn, L. B. F. Juurlink, and G.-J. Kroes, "Anomalous dependence of the reactivity on the presence of steps: Dissociation of D_2 on Cu(211)," J. Phys. Chem. Lett. **9**, 170–175 (2018).
[38]E. W. F. Smeets, G. Füchsel, and G.-J. Kroes, "Quantum dynamics of dissociative chemisorption of H_2 on the stepped Cu(211) surface," J. Phys. Chem. C **123**, 23049–23063 (2019).
[39]J. M. Boereboom, M. Wijzenbroek, M. F. Somers, and G. J. Kroes, "Towards a specific reaction parameter density functional for reactive scattering of H_2 from Pd(111)," J. Chem. Phys. **139**, 244707 (2013).
[40]G. Wiesenekker, G. J. Kroes, E. J. Baerends, and R. C. Mowrey, "Dissociation of H_2 on Cu(100): Dynamics on a new two-dimensional potential energy surface," J. Chem. Phys. **102**, 3873–3883 (1995).
[41]N. Pineau, H. F. Busnengo, J. C. Rayez, and A. Salin, "Relaxation of hot atoms following H_2 dissociation on a Pd(111) surface," J. Chem. Phys. **122**, 214705 (2005).
[42]M. S. Daw and M. I. Baskes, "Semiempirical quantum mechanical calculation of hydrogen embrittlement in metals," Phys. Rev. Lett. **50**, 1285–1288 (1983).
[43]M. J. Stott and E. Zaremba, "Quasiatoms: An approach to atoms in nonuniform electronic systems," Phys. Rev. B **22**, 1564–1583 (1980).
[44]J. K. Nørskov, "Covalent effects in the effective-medium theory of chemical binding: Hydrogen heats of solution in the 3D metals," Phys. Rev. B **26**, 2875–2885 (1982).
[45]M. S. Daw and M. I. Baskes, "Embedded-atom method: Derivation and application to impurities, surfaces, and other defects in metals," Phys. Rev. B **29**, 6443–6453 (1984).
[46]Y.-F. Mo, "Molecular dynamics study on microstructural evolution during crystallization of rapidly supercooled zirconium melts," J. Alloys Compd. **688**, 654 (2016).
[47]K. M. Ridings, T. S. Aldershof, and S. C. Hendy, "Surface melting and breakup of metal nanowires: Theory and molecular dynamics simulation," J. Chem. Phys. **150**, 094705 (2019).
[48]Z. Hou, Q. Xiao, Z. Wang, J. Wang, R. Liu, and C. Wang, "Effect of twin boundary spacing on the deformation behaviour of Au nanowire," Physica B **581**, 411952 (2020).
[49]C. O. T. Galvin, "A molecular dynamics method to identify the liquidus and solidus in a binary phase diagram," Comput. Mater. Sci. **186**, 110016 (2021).
[50]B. Hammer, L. B. Hansen, and J. K. Nørskov, "Improved adsorption energetics within density-functional theory using revised Perdew–Burke–Ernzerhof functionals," Phys. Rev. B **59**, 7413–7421 (1999).
[51]J. P. Perdew, K. Burke, and M. Ernzerhof, "Generalized gradient approximation made simple," Phys. Rev. Lett. **77**, 3865–3868 (1996).
[52]J. Klimeš, D. R. Bowler, and A. Michaelides, "Chemical accuracy for the van der Waals density functional," J. Phys.: Condens. Matter **22**, 022201 (2010).
[53]C. C. Marston and G. G. Balint-Kurti, "The Fourier grid Hamiltonian method for bound state eigenvalues and eigenfunctions," J. Chem. Phys. **91**, 3571–3576 (1989).
[54]F. R. Kroeger and C. A. Swenson, "Absolute linear thermal-expansion measurements on copper and aluminum from 5 K to 320 K," J. Appl. Phys. **48**, 853–864 (1977).
[55]K. H. Chae, H. C. Lu, and T. Gustafsson, "Medium-energy ion-scattering study of the temperature dependence of the structure of Cu(111)," Phys. Rev. B **54**, 14082–14086 (1996).
[56]R. Bulirsch and J. Stoer, "Numerical treatment of ordinary differential equations by extrapolation methods," Numer. Math. **8**, 1–13 (1966).
[57]V. F. Sears and S. A. Shelley, "Debye–Waller factor for elemental crystals," Acta Crystallogr., Sect. A **47**, 441–446 (1991).
[58]H. J. C. Berendsen, J. P. M. Postma, W. F. van Gunsteren, A. DiNola, and J. R. Haak, "Molecular dynamics with coupling to an external bath," J. Chem. Phys. **81**, 3684–3690 (1984).
[59]*Dynamics of Gas-Surface Interactions: Atomic-Level Understanding of Scattering Processes at Surfaces*, Springer Series in Surface Sciences, edited by R. D. Muino and H. F. Busnengo (Springer-Verlag, Berlin, Heidelberg, 2013).
[60]G.-J. Kroes, J. I. Juaristi, and M. Alducin, "Vibrational excitation of H_2 scattering from Cu(111): Effects of surface temperature and of allowing energy exchange with the surface," J. Phys. Chem. C **121**, 13617–13633 (2017).
[61]M. Dohle and P. Saalfrank, "Surface oscillator models for dissociative sticking of molecular hydrogen at non-rigid surfaces," Surf. Sci. **373**, 14 (1996).
[62]Z. S. Wang, G. R. Darling, and S. Holloway, "The surface temperature dependence of the inelastic scattering and dissociation of hydrogen molecules from metal surfaces," J. Chem. Phys. **120**, 2923–2933 (2004).
[63]M. Wijzenbroek and G. J. Kroes, "An *ab initio* molecular dynamics study of D_2 dissociation on CO-precovered Ru(0001)," Phys. Chem. Chem. Phys. **18**, 21190–21201 (2016).
[64]M. Bonfanti, M. F. Somers, C. Díaz, H. F. Busnengo, and G.-J. Kroes, "7D quantum dynamics of H_2 scattering from Cu(111): The accuracy of the phonon sudden approximation," Z. Phys. Chem. **227**, 139–1420 (2013).
[65]G. Henkelman and H. Jónsson, "Theoretical calculations of dissociative adsorption of CH_4 on an Ir(111) surface," Phys. Rev. Lett. **86**, 664–667 (2001).
[66]L. Verlet, "Computer "experiments" on classical fluids. I. Thermodynamical properties of Lennard-Jones molecules," Phys. Rev. **159**, 98–103 (1967).
[67]D. H. Tsai, "The virial theorem and stress calculation in molecular dynamics," J. Chem. Phys. **70**, 1375–1382 (1979).
[68]L. Sementa, M. Wijzenbroek, B. J. van Kolck, M. F. Somers, A. Al-Halabi, H. F. Busnengo, R. A. Olsen, G. J. Kroes, M. Rutkowski, C. Thewes, N. F. Kleimeier, and H. Zacharias, "Reactive scattering of H_2 from Cu(100): Comparison of dynamics calculations based on the specific reaction parameter approach to density functional theory with experiment," J. Chem. Phys. **138**, 044708 (2013).